Research Square

Preprints are preliminary reports that have not undergone peer review.
They should not be considered conclusive, used to inform clinical practice,
or referenced by the media as validated information.

Short-TR Optimization on Post-Contrast Deep Learning Synthetic MRI (DL-MAGiC) for Improved Visualization of ACTH-Secreting Pituitary Microadenomas: A Technical Feasibility Study

Haili Chen
Traditional Chinese medicine hospital dianjiang Chongqing
Feng Li
Traditional Chinese medicine hospital dianjiang Chongqing
Pan Hu
Traditional Chinese medicine hospital dianjiang Chongqing
Hui You
Peking Union Medical College Hospital, Chinese Academy of Medical Sciences and Peking Union Medical College
Lin Lu
Peking Union Medical College Hospital, Chinese Academy of Medical Sciences and Peking Union Medical College
Lian Duan
Peking Union Medical College Hospital, Chinese Academy of Medical Sciences and Peking Union Medical College
Kan Deng
Peking Union Medical College Hospital, Chinese Academy of Medical Sciences and Peking Union Medical College
Yong Yao
Peking Union Medical College Hospital, Chinese Academy of Medical Sciences and Peking Union Medical College
Huijuan Zhu
Peking Union Medical College Hospital, Chinese Academy of Medical Sciences and Peking Union Medical College
Feng Feng
Traditional Chinese medicine hospital dianjiang Chongqing
Bo Hou
houbo97@pumch.cn

Peking Union Medical College Hospital, Chinese Academy of Medical Sciences and Peking Union Medical College

Research Article

Keywords: Cushing disease, ACTH-secreting pituitary microadenoma, Synthetic MRI, MAGiC, Repetition time

Posted Date: August 31st, 2026

DOI: https://doi.org/10.21203/rs.3.rs-10763960/v1

License: This work is licensed under a Creative Commons Attribution 4.0 International License. Read Full License

Additional Declarations: No competing interests reported.

Abstract

Objective

To determine the optimal post-contrast TR/TE settings on deep learning synthetic MRI (DL-MAGiC) for maximizing visualization of ACTH-secreting pituitary microadenomas in Cushing disease.

Materials and Methods

This single-center prospective cohort study included 49 patients (hypoenhancing, n = 42; hyperenhancing, n = 7) with ACTH-secreting pituitary microadenomas who underwent post-contrast 1-mm DL-MAGiC imaging. Sixteen TR/TE combinations (TR: 100, 300, 500, 700 ms; TE: 5, 8, 14, 20 ms) were synthesized, and contrast-to-noise ratio (CNR) and signal-to-noise ratio (SNR) were compared using two-way repeated-measures analysis of variance. Qualitative assessment was independently performed by two blinded readers on five representative TR/TE combinations using a 5-point Likert scale for lesion conspicuity and boundary delineation; interobserver agreement was assessed with weighted kappa statistics.

Results

In hypoenhancing lesions, short TR (100–300 ms) significantly increased CNR versus long TR (500–700 ms) across all TE values (P<.001), with peak CNR at 100/8 ms (9.63 ± 5.94 vs 5.15 ± 3.83 at 700/20 ms, + 87%). The accompanying decreases in adenoma and gland SNR were modest (approximately 25% and 1%, respectively). TE had limited effect. In the hyperenhancing subgroup (n = 7), no significant TR/TE effects were seen. Qualitative scores were highest at 100/5–8 ms for both phenotypes.

Conclusion

Short-TR optimization (100 ms, TE 5–8 ms) on post-contrast DL-MAGiC improves CNR and conspicuity of hypoenhancing ACTH-secreting microadenomas with only modest SNR loss. These findings provide a technical reference for synthetic MRI post-processing; diagnostic performance studies are warranted to establish clinical utility.

INTRODUCTION

Magnetic resonance imaging (MRI) is the reference standard for detecting ACTH-secreting pituitary microadenomas in Cushing disease (CD). However, conventional MRI protocols fail to identify the causative lesion in approximately 40% of cases, primarily due to insufficient contrast between the adenoma and the avidly enhancing normal pituitary gland.[1–6].Accurate preoperative localization of these adenomas is crucial for determining optimal treatment strategies and predicting clinical outcomes, as failed localization may lead to delayed treatment, repeated imaging, or even bilateral adrenalectomy. [7]

Although shortening TR and TE can enhance T1 contrast between tumor and gland tissue, [8, 9] conventional MRI does not permit parameter modification after acquisition, making iterative protocol optimization clinically impractical. This constraint is particularly limiting for pituitary imaging, where the optimal TR/TE combination may vary depending on individual tumor enhancement characteristics and must be balanced against scan time and signal-to-noise ratio (SNR) considerations.

The magnetic resonance image compilation (MAGiC) sequence overcomes this limitation by acquiring quantitative T1, T2, and proton density maps in a single scan, enabling retrospective synthesis of contrast-weighted images at arbitrary TR/TE combinations without rescanning .[10–13] When combined with deep learning-based reconstruction, this approach achieves high-resolution thin-slice imaging with preserved signal quality.[14, 15] However, MAGiC has not been applied to pituitary microadenoma detection. Moreover, ACTH-secreting adenomas exhibit heterogeneous post-contrast enhancement patterns, broadly classified as hypoenhancing or hyperenhancing relative to the normal gland, and no study has evaluated whether optimal synthetic TR/TE parameters differ between these enhancement phenotypes. This gap is clinically significant because hypoenhancing adenomas—the more common phenotype—are precisely those most likely to be missed on conventional imaging due to inadequate lesion-to-gland contras. [16, 17]. Prior synthetic MRI research has focused on multiple sclerosis ,[18] head and neck pathology ,[11, 19, 20] and meningitis.[21]

Therefore, this study aimed to systematically optimize TR/TE settings on post-contrast deep learning MAGiC (DL-MAGiC) to maximize visualization across different enhancement phenotypes of ACTH-secreting pituitary microadenomas.

MATERIALS AND METHODS

Study Design and Patient Selection

This single-center prospective observational technical study was approved by the Institutional Review Board of Peking Union Medical College Hospital, and the requirement for written informed consent was waived. Between August 2024 and January 2025, 71 consecutive patients with a clinical diagnosis of Cushing disease (CD) were enrolled. All patients underwent precontrast conventional pituitary MRI followed by post-contrast coronal T1-weighted fast spin echo (FSE) and MAGiC sequences.

Inclusion required surgical resection with pathologic confirmation of an ACTH-secreting pituitary adenoma. Exclusion criteria were as follows: (1) absence of pathologic confirmation of an ACTH-secreting adenoma (n = 20); and (2) pathologic diagnosis of a non-ACTH pituitary adenoma (n = 2). The final cohort comprised 49 patients, including 29 women (59%), with a median age of 39 years (interquartile range [IQR], 28–53 years).Sample size was determined by consecutive enrollment of all eligible patients during the study period; no formal a priori power calculation was performed, as this was an exploratory technical feasibility study.

MRI Acquisition

All examinations were performed on a 3.0-T scanner (SIGNA Premier; GE HealthCare) with a 48-channel head coil. The protocol included precontrast coronal T1-weighted, coronal T2-weighted, and sagittal T1-weighted imaging. Gadobutrol (Gadovist; Bayer HealthCare) was administered intravenously at a dose of 0.1 mmol/kg body weight at 2 mL/s, followed by a 10-mL saline flush. Post-contrast sequences included coronal three-dimensional (3D) T1-weighted FSE (1-mm slice thickness, fat-saturated) and the MAGiC sequence (1-mm slice thickness). Deep learning-based reconstruction was applied to all sequences. Detailed acquisition parameters are listed in Table 1.

Table 1
MRI Acquisition Parameters

Sequence	TR/TE(ms)	FOV(cm^2)	Slice thickness/spacing(mm)	Number of slices	ETL	NEX	Matrix	Scan time(s)
Coronal 2D FSE T2WI	4100//90	20×20	4/1	20	3	1.2	32×320	49
Coronal 2D FSE T1W	400/12	18×16.2	3/0.6	10	3	2	256×192	49
CE coronal FS 3D FSE T1WI	350/16	18×18	1/0	20	3	2	300×200	90
CE MAGiC	4000/12.6	19.5×18	1/0.2	20	14		272×192	336

Abbreviations: CE, contrast-enhanced; ETL, echo train length; FS, fat-saturated; FSE, fast spin echo; NEX, number of excitations.

Image Post-Processing and Quantitative Image Analysis

Post-contrast 3D T1-weighted FSE images served as anatomic references for lesion localization. Synthetic T1-weighted images were generated at 16 TR/TE combinations (TR: 100, 300, 500, 700 ms; TE: 5, 8, 14, 20 ms) on the MRI scanner host console, selected based on published parameter ranges for pituitary T1-weighted imaging and software constraints.[8, 22, 23] All quantitative measurements were performed independently by two radiology technologists (with 15 and 8 years of MR experience, respectively) who were blinded to clinical information.

On each synthesized image, regions of interest (ROIs) were manually placed at the lesion's largest cross-sectional area. Adenoma ROIs were placed in the solid tumor component, carefully avoiding areas of liquefaction, necrosis, or hemorrhage. Normal pituitary ROIs were placed in the anterior lobe, and background noise ROIs were placed in air along the phase-encoding direction. ROI geometry and position were kept identical across all 16 parameter combinations (Fig. 1).

Quantitative metrics were calculated as follows:

$$CNR = |SI(\text{normal pituitary}) - SI(\text{adenoma})| / SD(\text{background noise})$$

$$SNR(\text{adenoma}) = SI(\text{adenoma}) / SD(\text{background noise})$$

$$SNR(\text{gland}) = SI(\text{normal pituitary}) / SD(\text{background noise})$$

where SI denotes signal intensity and SD denotes standard deviation.

Enhancement Pattern Classification

ACTH-secreting pituitary microadenomas were classified into two enhancement phenotypes—hypoenhancing and hyperenhancing—based on the signal intensity ratio (SI ratio). The SIratio was defined as adenoma signal intensity divided by normal anterior pituitary signal intensity, measured at conventional pituitary imaging parameters (TR = 500 ms, TE = 14 ms). Receiver operating characteristic analysis yielded an area under the curve of 0.992 ($P < .05$), with an optimal cutoff of 1.210. Lesions with SIratio < 1.210 were classified as hypoenhancing (n = 42), and those with SIratio ≥ 1.210 as hyperenhancing (n = 7) .

Qualitative Assessment of Lesion Visualization

Two radiologists with 25 and 16 years of experience in neuroradiology, who were blinded to the clinical data and final diagnoses, independently performed the qualitative assessment. Before formal assessment, both readers underwent a dedicated training session to standardize scoring criteria.

Five representative TR/TE combinations were selected for qualitative evaluation: 100/5 ms, 100/8 ms, 300/8 ms, 500/14 ms, and 700/20 ms, representing optimal (100/5, 100/8), intermediate (300/8), and conventional (500/14, 700/20) CNR performance.

Two domains were independently rated on a 5-point Likert scale: (1) lesion conspicuity, defined as the perceptibility of the adenoma against the surrounding normal pituitary gland; and (2) boundary delineation, defined as the sharpness of the lesion–gland interface. Scoring criteria were as follows: 5 = excellent (lesion clearly distinguishable with sharp margins); 4 = good (good contrast with moderately sharp margins); 3 = fair (lesion discernible with acceptable but suboptimal contrast and margin sharpness); 2 = poor (lesion barely visible with blurred margins, but still discernible); and 1 = nondiagnostic (lesion nearly invisible or indistinguishable from the normal gland). Disagreements were resolved by consensus or adjudication by a third senior radiologist (> 20 years of experience).

Bias Control

Several measures were implemented to minimize potential bias. First, all quantitative ROI measurements were performed independently by two radiology technologists blinded to clinical information. Second, the two neuroradiologists who performed qualitative assessment were blinded to clinical data. Third, the five TR/TE combinations for qualitative evaluation were presented in a randomized order to avoid expectation bias. Fourth, ROI geometry and position were kept identical across all 16 parameter combinations to ensure consistency.

Statistical Analysis

Statistical analyses were performed using GraphPad Prism (version 9.5.1) and R (version 4.4.2). Quantitative data are expressed as mean ± standard deviation. Two-way repeated-measures analysis of variance (ANOVA) assessed the main effects of TR and TE and their interaction on CNR and SNR. When significant main effects or interactions were identified, post hoc pairwise comparisons were performed using paired t-tests with Bonferroni correction. Inter-observer agreement for the qualitative scores was evaluated using weighted kappa statistics (κ) with quadratic weights and interpreted as follows: >0.81, almost perfect; 0.61–0.80, substantial; 0.41–0.60, moderate; 0.21–0.40, fair; and < 0.20, poor. A two-sided P < 0.05 was considered statistically significant. No missing data were present for the primary analyses.

RESULTS

Quantitative Image Analysis

In the hypoenhancing group, CNR was highest at TR/TE = 100/8 ms (9.63 ± 5.94) and TR/TE = 100/5 ms (8.48 ± 4.95), representing increase of 87.0% and 64.7%, respectively, compared with that at TR/TE = 700/20 ms (5.15 ± 3.83) (*P* < .001). Adenoma SNR progressively decreased with shorter TR, from 13.24 ± 3.86 at TR/TE = 700/20 ms to 9.78 ± 3.98 at TR/TE = 100/5 ms corresponding to an approximately 25% reduction. In contrast, gland SNR remained relatively stable across all TR/TE combinations (range, 18.26 ± 8.35 to 20.29 ± 9.29) (Table 2). TE variation produced statistically significant (*P* < .001) but quantitatively small differences in CNR, adenoma SNR, and gland SNR, primarily between TE = 5 ms and longer TE values. ANOVA analysis confirmed that TR exerted a substantially greater effect on CNR than TE .

Table 2
Quantitative image quality metrics across representative synthetic TR/TE combinations

TR/TE (ms)	Hypoenhancing group (n = 42)			Hyperenhancing group (n = 7)		
	CNR	SNR (adenoma)	SNR (gland)	CNR	SNR (adenoma)	SNR (gland)
100/5	8.48 ± 4.95	9.78 ± 3.98	18.26 ± 8.35	1. 37 ± 5.78	13.47 ± 6.33	12.10 ± 6.45
100/8	9.63 ± 5.94	10.65 ± 4.58	20.29 ± 9.29	1.68 ± 6.34	15.5 ± 11.62	13.91 ± 8.55
300/8	8.04 ± 4.79	10.91 ± 4.49	18.95 ± 7.91	1.30 ± 4.98	14.94 ± 10.35	13.63 ± 7.79
500/14	5.72 ± 4.42	12.28 ± 4.28	18.01 ± 5.96	-0.88 ± 3.93	17.28 ± 8.26	16.40 ± 6.12
700/20	5.15 ± 3.83	13.24 ± 3.86	18.39 ± 5.00	-1.34 ± 4.36	17.66 ± 8.49	16.56 ± 6.25
TR main effect P value	< 0.001	< 0.001	< 0.05	> 0.05	> 0.05	> 0.05

In the hyperenhancing group, CNR values demonstrated substantial inter-individual variability across all tested TR/TE combinations, with mean CNR ranging from − 1.34 ± 4.36 at TR = 700/20 ms to 1.68 ± 6.34 at TR = 100/8 ms (Table 2). Neither TR nor TE significantly altered CNR or SNR (all *P* > .05), with the sole exception of a significant difference between TE = 5 ms and TE = 20 ms (*P* < .05). The large standard deviations reflect the small sample size and inherent biological variability within this subgroup. Given the exploratory nature of this subgroup analysis, these findings should be interpreted with caution. All statistical analyses results are presented in Fig. 2 and Fig. 3.

Lesion Visualization

Qualitative assessment of the five selected TR/TE combinations demonstrated a progressive decline in lesion conspicuity and boundary delineation with increasing TR. At TR = 100/5 ms and 100/8 ms, both hypoenhancing and hyperenhancing lesions received the highest scores (median = 5.0), although boundary delineation at 100/8 ms showed slightly greater variability (IQR, 4.0–5.0) than lesion conspicuity (IQR, 5.0–5.0) (Fig. 4a-b and Fig. 5a-b). At TR = 300/8 ms, median scores declined to 4.0 for both domains (Fig. 4c and Fig. 5c). A further decline was observed at longer TR/TE settings, with median scores of 3.0 at TR/TE = 500/14 ms and 2.0 at TR/TE = 700/20 ms (Fig. 4d–e and 5d–e). Interobserver agreement was almost perfect for short-TR settings (weighted κ = 0.89–0.91) and substantial for long-TR settings (weighted κ = 0.72–0.80) (Table 3).

Table 3
Qualitative Assessment Scores Across Five Representative TR/TE Combinations

TR/TE (ms)	Lesion Conspicuity Median (IQR)	Boundary Delineation Median (IQR)	Weighted κ (95% CI)
100/5	5.0 (4.0–5.0)	5.0 (4.0–5.0)	0.89 (0.82–0.94)
100/8	5.0 (5.0–5.0)	5.0 (4.0–5.0)	0.91 (0.85–0.96)
300/8	4.0 (3.0–4.0)	4.0 (3.0–4.0)	0.86 (0.78–0.92)
500/14	3.0 (2.0–3.0)	3.0 (2.0–3.0)	0.80 (0.70–0.88)
700/20	2.0 (1.0–2.0)	2.0 (1.0–2.0)	0.72 (0.60–0.82)
Abbreviations: IQR, interquartile range; CI, confidence interval.			
Scoring: 5 = excellent; 4 = good; 3 = fair; 2 = poor; 1 = nondiagnostic.			
Weighted κ interpretation: 0.81–1.00 = almost perfect; 0.61–0.80 = substantial; 0.41–0.60 = moderate.			

DISCUSSION

In this study, short-TR optimization on post-contrast DL-MAGiC significantly improved CNR and qualitative lesion visualization in hypoenhancing ACTH-secreting pituitary microadenomas. By systematically evaluating 16 synthetic TR/TE combinations, we identified TR = 100 ms with TE = 5–8 ms as the optimal setting for maximizing lesion-to-gland contrast. It should be emphasized that this investigation was designed as a technical feasibility study to characterize signal behavior and contrast optimization, rather than a diagnostic performance study. As such, the findings provide a parameter-selection reference rather than a clinical diagnostic endorsement.

The observed CNR gain with short TR is consistent with the physics of T1-weighted imaging. TR determines the extent of longitudinal magnetization recovery between excitation pulses, and shorter TR values preferentially suppress signal from tissues with longer T1 relaxation times. After gadolinium administration, the normal pituitary gland typically undergoes greater T1 shortening than the less-enhancing adenoma because of its rich vascularity and avid contrast uptake. Under short TR conditions, this difference amplifies the signal separation between gland and lesion, thereby increasing CNR. [8]. By contrast, TE primarily influences T2-related signal decay and therefore plays a secondary role in post-contrast T1-weighted contrast generation, which explains its comparatively limited influence in the present study.

Our findings extend those of Chowdhury et al. [9] who demonstrated that reducing TR from > 492 ms to 401 ms in conventional FSE imaging (with TE of 9–10 ms) enabled detection of previously occult ACTH-secreting tumors. The present study advances this concept by demonstrating further CNR improvement down to TR = 100 ms, a parameter range inaccessible to conventional FSE acquisitions due to scan time constraints but is readily achievable through MAGiC synthesis. Because MAGiC operates through multi-echo, multi-delay acquisitions and quantitative map-based reconstruction, synthesized images generated at short TR reflect effective T1 contrast, which differ from conventional single-echo FSE acquisitions. This concept parallels the effective relaxation time (T_2, eff) framework described by Kim et al. [24] in prostate FSE imaging, where signal behavior in multi-echo sequences deviates from conventional spin echo predictions. Similarly, the CNR improvement observed at short synthetic TR likely reflects optimization of effective T1 contrast (T_1,eff) within the MAGiC acquisition framework.

A recognized limitation of synthetic MRI is its lower SNR compared with conventional acquisitions. [13]. In the present study, although short TR was associated with a modest reduction in SNR, this decrease did not compromise lesion

identification. This preservation of diagnostic image quality may be attributable to DL-based reconstruction, which has been shown to mitigate noise amplification associated with both thin-slice imaging and short-TR synthesis. [15, 25, 26] In clinical practice, microadenoma detection depends more on lesion-to-gland contrast than on absolute signal intensity; therefore, the CNR gain achieved with short TR is likely to outweigh the accompanying modest SNR penalty.

The classification of ACTH-secreting adenomas into hypoenhancing and hyperenhancing phenotypes addresses a potential source of heterogeneity that has been insufficiently considered in prior pituitary imaging studies. The significant benefit of TR optimization in hypoenhancing lesions, but not in hyperenhancing lesions, is clinically meaningful because hypoenhancing adenomas constituted the majority of our cohort (86%, 42/49) and are also the lesions most likely to be missed on routine imaging. These findings suggest that short TR optimization may be particularly valuable in diagnostically challenging cases and that enhancement phenotype should be considered in future imaging studies of Cushing disease.

The translational implication of our findings also deserve emphasis. The optimal parameters identified through MAGiC post-processing (TR = 100 ms, TE = 5–8 ms) may inform further refinement of conventional pituitary MRI protocols. More broadly, DL-MAGiC represents a flexible imaging approach that integrates high spatial resolution, retrospectivle contrast optimization, and DL-enhanced image quality, which may be valuable for detecting other small lesions in neuroimaging and beyond.

We optimized TR/TE parameters using DL-MAGiC in this study, but we did not go on to test these optimized settings directly on the conventional FSE sequence. That kind of validation is something we have planned for our next study. For now, CNR and Likert scores are not perfect measures, but they serve well as endpoints for a signal-optimization effort at this stage. What we intend to do next is a formal diagnostic comparison, where we will apply the optimal synthetic parameters to conventional FSE and look at lesion detection, sensitivity, and specificity. That will need a dedicated prospective design and enough statistical power to give meaningful results.

This study has several limitations. First, we did not directly validate the optimized parameters on the conventional FSE sequence, so CNR and Likert scores remain surrogate endpoints rather than direct evidence of diagnostic improvement. A formal comparison of the two approaches will be needed to establish clinical utility. Second, this was a single-center study with a modest sample size, and the hyperenhancing subgroup in particular included only seven patients, which limits statistical power and generalizability. Third, the cutoff used to classify hypoenhancing and hyperenhancing lesions was derived from the same cohort used for optimization; while this is acceptable for a preliminary study, it still requires validation in an independent dataset. We also acknowledge that our findings are specific to ACTH-secreting microadenomas and may not apply to other sellar lesions. Future work should involve larger, preferably multicenter cohorts with external validation and blinded diagnostic testing to confirm these results.

CONCLUSION

Short TR optimization on post contrast DL-MAGiC significantly boosts CNR and conspicuity for hypoenhancing ACTH-secreting microadenomas. Our data provide a useful technical reference for synthetic MRI parameter selection in this challenging condition. Still, clinical translation will require a formal diagnostic study, with blinding and conventional FSE as the comparator, to determine whether the improved signal translates into better detection and localization in practice.

Declarations

Author Contribution

H.C., F.L., and P.H. contributed equally to this work and share first authorship. They conceived and designed the study and wrote the main manuscript. L.L., L.D., H.Z., K.D., and Y.Y. participated in the collection and clinical interpretation of patient data. Quantitative measurements were independently performed by H.C. and B.H., who have 8 and 15 years of MR experience, respectively, and were blinded to clinical information. Image interpretation was carried out by F.F. and H.Y., who have 25 and 16 years of experience in neuroradiology, respectively, and were blinded to clinical data and final diagnoses. F.F. and B.H. critically revised the manuscript for important intellectual content and provided overall supervision. All authors reviewed and approved the final version of the manuscript.

Data Availability

The raw MRI data and clinical patient information generated and analyzed during this study are not publicly available due to patient privacy protection and institutional regulations. The datasets used and/or analyzed during the current study are available from the corresponding author (Bo Hou, houbo97@pumch.cn) upon reasonable request, subject to approval from the Institutional Review Board of Peking Union Medical College Hospital and the signing of appropriate data-sharing agreements.

References

1. Honegger J, Nasi-Kordhishti I, Giese S (2019) Hypophysenadenome Nervenarzt 90:568–577. https://doi.org/10.1007/s00115-019-0708-4
2. Nishioka H, Yamada S (2019) Cushing's disease. J Clin Med 8:1951. https://doi.org/10.3390/jcm8111951
3. Kasaliwal R, Sankhe SS, Lila AR et al (2013) Volume interpolated 3D-spoiled gradient echo sequence is better than dynamic contrast spin echo sequence for MRI detection of corticotropin secreting pituitary microadenomas. Clin Endocrinol 78:825–830. https://doi.org/10.1111/cen.12069
4. Mahmoud OM, Tominaga A, Amatya VJ et al (2011) Role of PROPELLER diffusion-weighted imaging and apparent diffusion coefficient in the evaluation of pituitary adenomas. Eur J Radiol 80:412–417. https://doi.org/10.1016/j.ejrad.2010.05.023
5. Lien RJ, Corcuera-Solano I, Pawha PS et al (2015) Three-tesla imaging of the pituitary and parasellar region: T1-weighted 3-dimensional fast spin echo cube outperforms conventional 2-dimensional magnetic resonance imaging. J Comput Assist Tomogr 39:787–793. https://doi.org/10.1097/RCT.0000000000000214
6. Kakite S, Fujii S, Kurosaki M et al (2011) Three-dimensional gradient echo versus spin echo sequence in contrast-enhanced imaging of the pituitary gland at 3T. Eur J Radiol 79:108–112. https://doi.org/10.1016/j.ejrad.2009.12.036
7. Liu Z, Hou B, You H et al (2024) Three-dimensional fast spin echo pituitary MRI in treatment-naïve Cushing's disease: reduced impact of reader experience and increased diagnostic accuracy. J Magn Reson Imaging 59:2115–2123. https://doi.org/10.1002/jmri.28975
8. Peck W, Dillon W, Norman D et al (1989) High-resolution MR imaging of pituitary microadenomas at 1.5 T: experience with Cushing disease. AJR Am J Roentgenol 152:145–151. https://doi.org/10.2214/ajr.152.1.145
9. Chowdhury IN, Sinaii N, Oldfield EH et al (2010) A change in pituitary magnetic resonance imaging protocol detects ACTH-secreting tumours in patients with previously negative results. Clin Endocrinol 72:502–506. https://doi.org/10.1111/j.1365-2265.2009.03646.x
10. Fujita S, Hagiwara A, Hori M et al (2019) 3D quantitative synthetic MRI-derived cortical thickness and subcortical brain volumes: scan-rescan repeatability and comparison with conventional T1-weighted images. J Magn Reson Imaging 50:1834–1842. https://doi.org/10.1002/jmri.26744

11. Ji S, Yang D, Lee J et al (2022) Synthetic MRI: technologies and applications in neuroradiology. J Magn Reson Imaging 55:1013–1025. https://doi.org/10.1002/jmri.27440
12. Wang P, Hu S, Wang X et al (2023) Synthetic MRI in differentiating benign from metastatic retropharyngeal lymph node: combination with diffusion-weighted imaging. Eur Radiol 33:152–161. https://doi.org/10.1007/s00330-022-09027-4
13. Di Giuliano F, Minosse S, Picchi E et al (2020) Comparison between synthetic and conventional magnetic resonance imaging in patients with multiple sclerosis and controls. Magn Reson Mater Phy 33:549–557. https://doi.org/10.1007/s10334-019-00804-9
14. Ishimoto Y, Ide S, Watanabe K et al (2024) Usefulness of pituitary high-resolution 3D MRI with deep-learning-based reconstruction for perioperative evaluation of pituitary adenomas. Neuroradiology 66:937–945. https://doi.org/10.1007/s00234-024-03315-0
15. Lee DH, Park JE, Nam YK et al (2021) Deep learning-based thin-section MRI reconstruction improves tumour detection and delineation in pre- and post-treatment pituitary adenoma. Sci Rep 11:21302. https://doi.org/10.1038/s41598-021-00558-2
16. Castle-Kirszbaum M, Amukotuwa S, Fuller P et al (2023) MRI for Cushing disease: a systematic review. AJNR Am J Neuroradiol 44:311–316. https://doi.org/10.3174/ajnr.A7789
17. Miki Y, Matsuo M, Nishizawa S et al (1990) Pituitary adenomas and normal pituitary tissue: enhancement patterns on gadopentetate-enhanced MR imaging. Radiology 177:35–38. https://doi.org/10.1148/radiology.177.1.2399335
18. Krauss W, Gunnarsson M, Nilsson M, Thunberg P (2018) Conventional and synthetic MRI in multiple sclerosis: a comparative study. Eur Radiol 28:1692–1700. https://doi.org/10.1007/s00330-017-5100-9
19. Konar AS, Paudyal R, Shah AD et al (2022) Qualitative and quantitative performance of magnetic resonance image compilation (MAGiC) method: an exploratory analysis for head and neck imaging. Cancers 14:3624. https://doi.org/10.3390/cancers14153624
20. Zhang Z, Li S, Wang W et al (2023) Synthetic MRI for the quantitative and morphologic assessment of head and neck tumors: a preliminary study. Dentomaxillofac Radiol 52:20230103. https://doi.org/10.1259/dmfr.20230103
21. Andica C, Hagiwara A, Nakazawa M et al (2017) Synthetic MR imaging in the diagnosis of bacterial meningitis. Magn Reson Med Sci 16:91–92. https://doi.org/10.2463/mrms.ci.2016-0082
22. Nichols DA, Laws ER, Houser OW, Abboud CF (1988) Comparison of magnetic resonance imaging and computed tomography in the preoperative evaluation of pituitary adenomas. Neurosurgery 22:380–385. https://doi.org/10.1227/00006123-198802000-00018
23. Kucharczyk W, Davis DO, Kelly WM et al (1986) Pituitary adenomas: high-resolution MR imaging at 1.5 T. Radiology 161:761–765. https://doi.org/10.1148/radiology.161.3.3786729
24. Kim D, Pabi R, Borisch EA et al (2026) Optimal Selection of the Effective Echo Time (TEeff) for T2 -Weighted Fast-Spin-Echo MRI of the Prostate at 3.0 T: Effect on Lesion Conspicuity. Magn Reson Imaging jmri 70351. https://doi.org/10.1002/jmri.70351
25. Wang X, Ma J, Bhosale P et al (2021) Novel deep learning-based noise reduction technique for prostate magnetic resonance imaging. Abdom Radiol 46:3378–3386. https://doi.org/10.1007/s00261-021-02964-6
26. Zhang K, Zuo W, Chen Y et al (2017) Beyond a Gaussian denoiser: residual learning of deep CNN for image denoising. IEEE Trans Image Process 26:3142–3155. https://doi.org/10.1109/TIP.2017.2662206

Figures

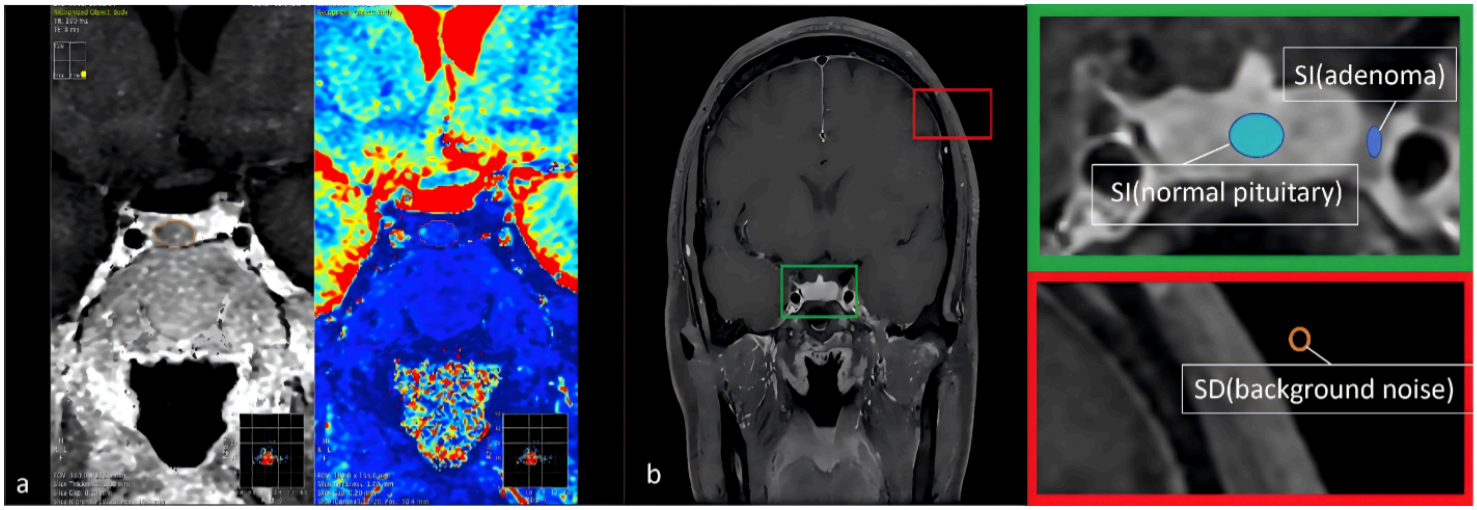


Figure 1

Post-contrast DL-MAGiC T1-weighted image and corresponding T1 map showing ROI placement for adenoma (dark blue), normal pituitary (light blue), and background noise (orange).

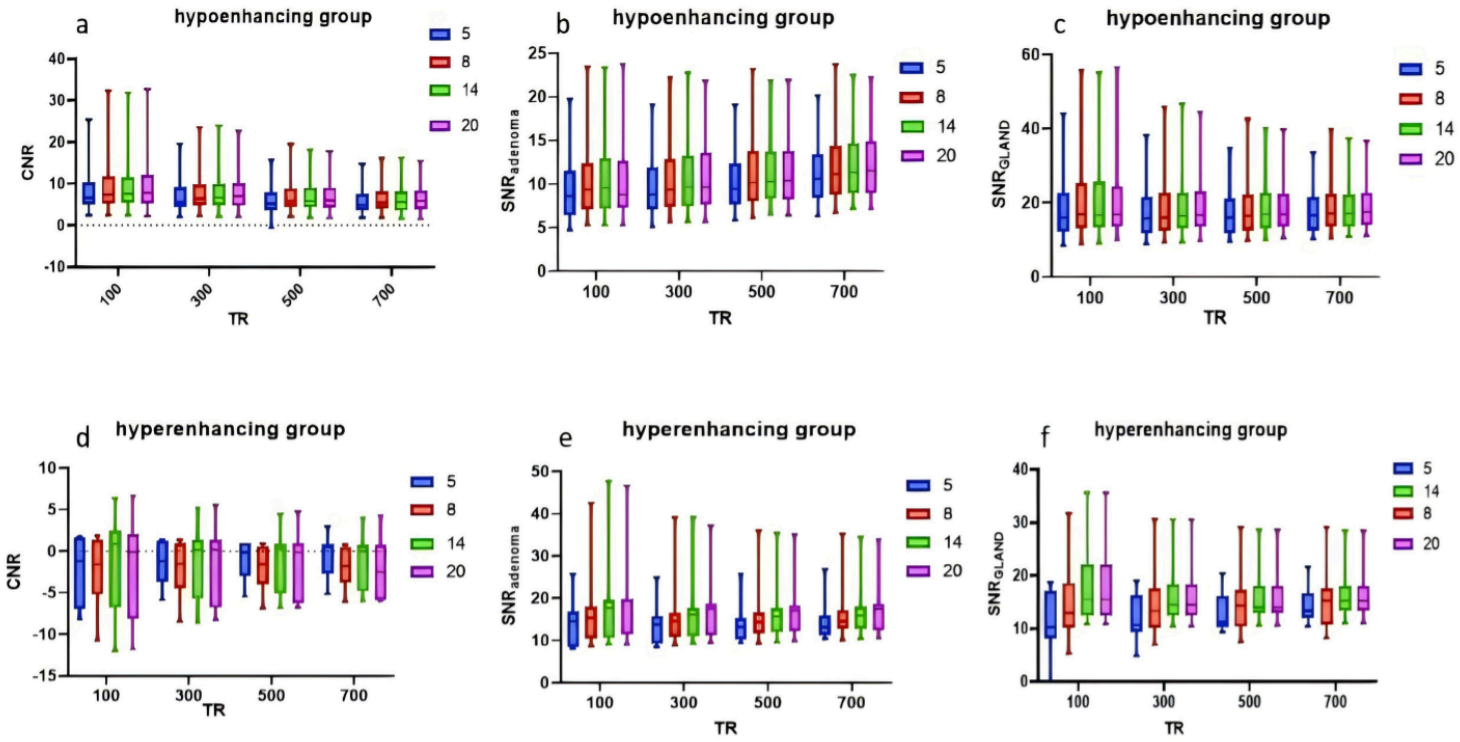


Figure 2

Effect of TR on CNR and SNR at fixed TE. In hypoenhancing adenomas, shorter TR significantly increases CNR (a), with corresponding SNR changes in adenoma (b) and normal gland (c). In hyperenhancing adenomas, CNR (d) and SNR (e, f) show no significant changes with TR.

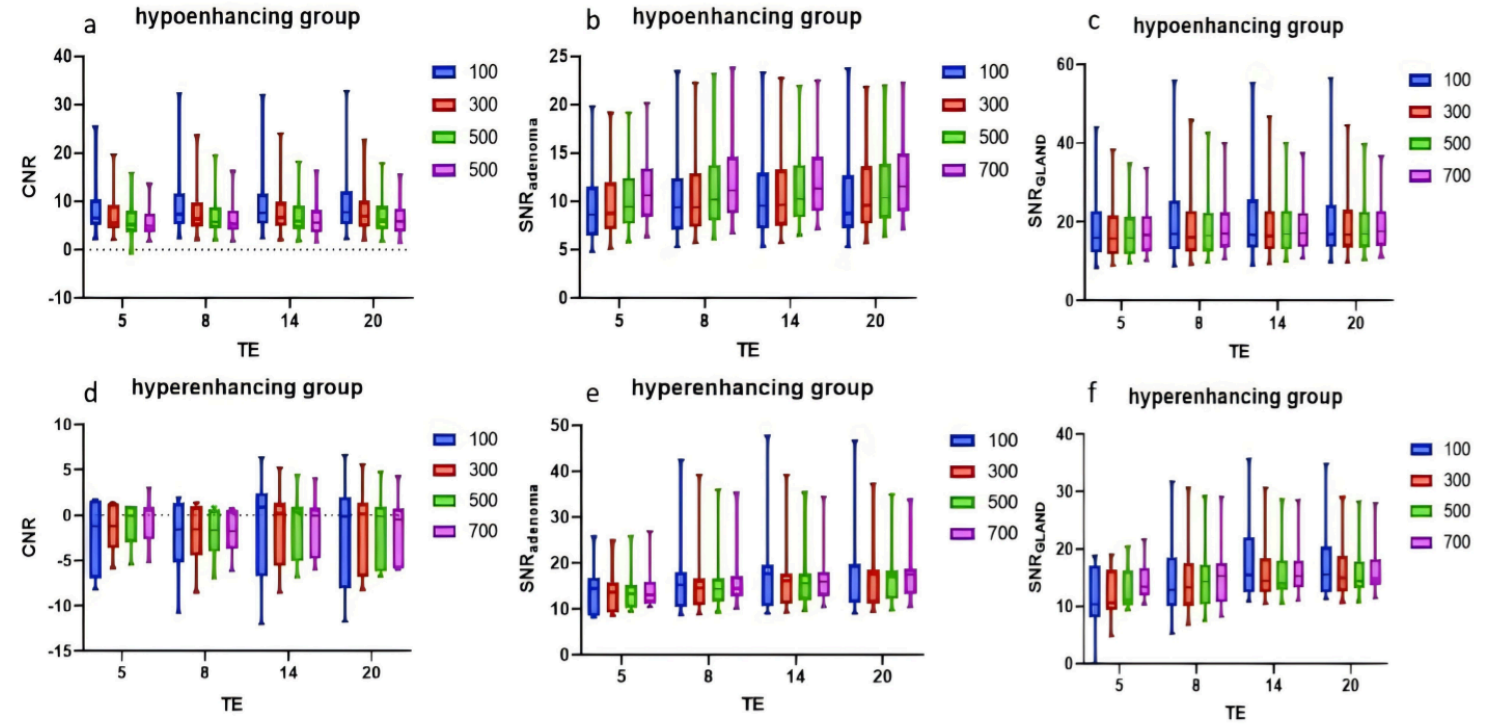


Figure 3

Effect of TE on CNR and SNR at fixed TR values. (a–c) Hypoenhancing group: TE variations produce statistically significant but quantitatively modest differences. (d–f) Hyperenhancing group: significant differences observed only between TE = 5 ms and TE = 20 ms.

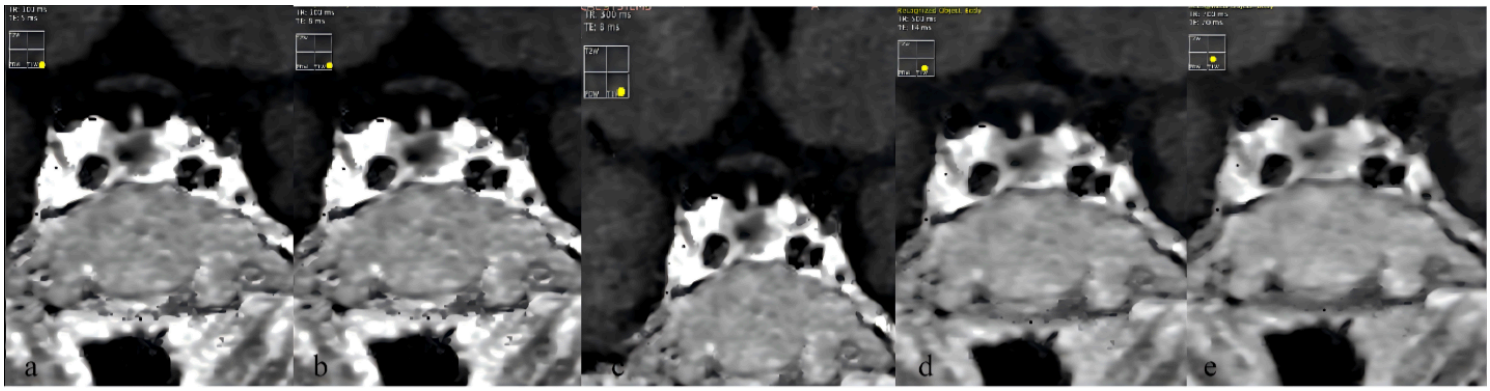


Figure 4

Representative images of a hypoenhancing ACTH-secreting microadenoma at five TR/TE combinations. Lesion conspicuity and margin sharpness progressively decline as TR increases from 100/5 ms (a) to 700/20 ms (e).

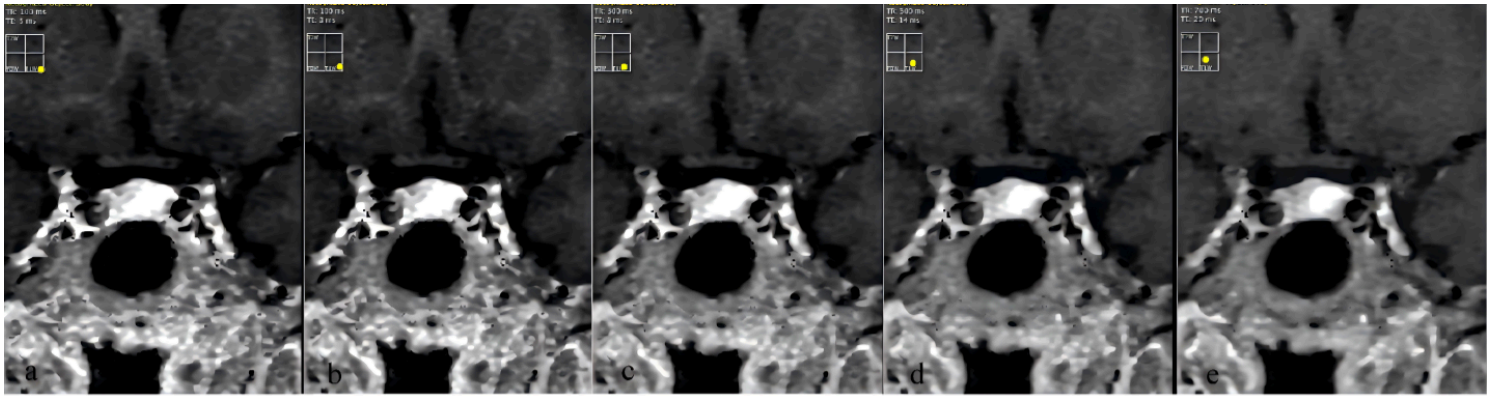


Figure 5

Representative images of a hyperenhaning ACTH-secreting microadenoma at five TR/TE combinations. Lesion visualization remains robust at short TR (a, b), but conspicuity and margin definition decrease with longer TR (c-e).